Overlapping internal boundary control of lane-free automated vehicle traffic

Milad Malekzadeh[a*], Venkata Karteek Yanumula[a], Ioannis Papamichail[a], Markos Papageorgiou[a,b]

[a]Dynamic Systems and Simulation Laboratory, Technical University of Crete, Chania 73100, Greece

[b]Faculty of Maritime and Transportation, Ningbo University, Ningbo, China

[*]Corresponding author (email: mmalek@dssl.tuc.gr)

Abstract

Lane-free vehicle driving has been recently proposed for connected automated vehicles on highways or arterials. Lane-free traffic implies that incremental changes of the road width lead to corresponding incremental changes of traffic flows and capacity. In these conditions, internal boundary control (IBC) was proposed for flexible sharing of the total road width and capacity among the two traffic directions of the highway in real-time in order to maximize the cross-road infrastructure utilization and minimize congestion and delays. Centralized solutions , e.g. LQ (linear quadratic) regulators, requiring information from the whole highway stretch under consideration, have already been proposed, which, however, may be cumbersome for long highways with respect to the offline controller design effort; the extent of real-time communications; and the physical system architecture. This paper investigates two different overlapping decentralized control schemes for IBC in lane-free automated vehicle traffic. The first approach is based on a contractible controller, which is designed and employed in a decomposed way, for each subsystem of an extended highway system. In the second approach, the overall discrete-time LQ control problem is transformed into a linear matrix inequalities (LMI) problem. After selecting the overlapping feedback structure and solving the overall LMI problem, the correspondingly structured gain matrix is obtained, enabling a decentralized overlapping control deployment in real-time. Simulation investigations, involving a realistic highway stretch and demand scenarios, demonstrate that the proposed decentralized regulators are almost as efficient as the centralized control solutions for the problem at hand.

Keywords: lane-free traffic, internal boundary control, linear-quadratic regulator, overlapping control, linear matrix inequalities (LMI).

1 Introduction

Road and highway traffic congestion is one of the most serious problems for big cities around the world, causing extensive delays, increased fuel consumption, excessive environmental pollution, and reduced traffic safety. Conventional traffic control measures are valuable (Papageorgiou et al. 2003; Kurzhanskiy and Varaiya, 2010), but not always sufficient to tackle the heavy traffic demand. Gradually emerging and future ground-breaking capabilities of connected automated vehicles (CAV) should be exploited to develop innovative solutions that can be applied to smart road infrastructures. Recently, there has been a strong interest in the scientific community in developing a variety of methods attempting to exploit current and future vehicle automation and communication systems for improved real-time traffic management, see e.g. (Diakaki et al., 2015; Papamichail et al., 2019) and references therein.

A novel paradigm for vehicular traffic, which is appropriate for high penetration rates of vehicles equipped with high-level automation and communication systems, was recently launched with the TrafficFluid concept (Papageorgiou et al., 2021), suggesting to abandon, in the CAV era, two main conventional restrictions that reflect physical limitations of human drivers. Specifically, the TrafficFluid concept suggests: (1) lane-free traffic, whereby vehicles are not bound to fixed traffic lanes, as in conventional traffic; (2) vehicle nudging, whereby vehicles may exert a "nudging" effect on, i.e. influence the movement of, vehicles in front of them.

In this context, it becomes possible to employ internal boundary control (IBC), a promising and innovative control measure aiming to achieve an unprecedented exploitation of the available road infrastructure (Malekzadeh et al. 2021a). It should be noted that IBC is facilitated by the first TrafficFluid feature, lane-free traffic, while vehicle nudging is not a prerequisite for IBC. More specifically, IBC relies on the fact that, in lane-free traffic, the traffic flow and capacity may exhibit incremental changes in response to corresponding incremental changes of the road width. Thus, on a highway or arterial with two opposite traffic directions, the total cross-road capacity (for both directions) may be shared between the two directions in real-time, according to the prevailing demand per direction, by virtually moving the internal boundary that separates the two traffic directions and communicating this decision to CAVs, so that they respect the changed road boundary. This calls for an appropriate real-time control strategy that changes the internal road boundary in space and time, as illustrated in Fig. 1, in response to the current traffic conditions, so as to maximize the traffic efficiency in both directions.

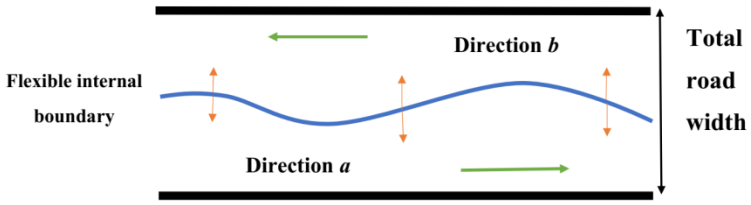

Fig. 1: Space-time flexible internal road boundary.

Real-time IBC for lane-free CAV traffic may be broadly applicable to the high number of arterial or highway infrastructures that feature unbalanced demands during the day in the two traffic directions, to strongly mitigate or even utterly suppress congestion. Even for infrastructures experiencing strong demand in both directions quasi-simultaneously, real-time IBC may intensify the road utilization and lead to sensible improvements.

The characteristics of IBC are analyzed by Malekzadeh et al. (2021a), where its high improvement potential is demonstrated by formulating and solving an open-loop optimal control problem, in the form of a convex Quadratic Programming (QP) problem, aiming at minimizing a physical criterion, the total time spent by all vehicles. That approach may be used within a Model Predictive Control (MPC) frame, with online demand prediction, for real-time application. However, simpler real-time approaches with similar efficiency, but without the need for online demand prediction, are preferable. Therefore, a feedback-based Linear-Quadratic Regulator (LQR) was developed by Malekzadeh et al. (2021b) for IBC, aiming at balancing the relative densities in the two directions; and have been demonstrated to be robust and similarly efficient as the open-loop optimal control solution, while avoiding the need for accurate modelling and external demand prediction. It is noteworthy that, for the needs of the present investigation, the two previously developed centralized strategies, QP and LQR, are applied here to different and, most importantly, more sizable highway systems than in (Malekzadeh, et al. 2021a) and (Malekzadeh, et al. 2021b).

However, for very long highways, the centralized LQR applying to the whole highway may have to be designed with hundreds of state variables; also, its application requires real-time information from the whole highway under consideration, which may be problematic for very long highways with respect to the required communications and physical system architecture. In other words, to calculate the control input (internal boundary position) at a specific highway location, the centralized LQR requires formally real-time information about the traffic conditions in the whole highway, i.e., even from highway parts that may be dozens of kilometers away, something that is obviously not necessary for efficient IBC operations.

Generally speaking, control decentralization in large-scale and geographically extended systems is a desirable and reasonable control structure, as it is simpler to monitor and maintain and more reliable in cases of device failures. Such features appear, for example, in the control of interconnected power systems (Patil et al. 2019), water systems (Hafeez et al. 2021), as well as in space or traffic systems (Pasquale et al. 2020), where analysis, synthesis and implementation is distributed to interacting subsystems (Siljak., 2011) under the motto "think global, act local". Such systems are typically composed of various physically or functionally local, possibly interacting control sub-stations, where each sub-station is in charge only of the operation of a part of the overall system, and the overall control system objective is reached by the actions of the local control subsystems.

Various methodologies were proposed in the past decades for the design of such decentralized control systems, the structure of which may be dictated by the structure of the process under control; or may have to be defined based on entailed performance, maintenance and communication requirements, reliability and other properties. In the latter case, there are four well-known system decomposition structures: disjoint decomposition, overlapping decomposition, border block diagonal decomposition, and epsilon decomposition (Bakule, 2014). The disjoint decomposition of the overall system is not reasonable if the subsystems are strongly interconnected, in which case an overlapping control structure may be employed, where the overlapping parts create connections between subsystems to enhance the local and overall control performance. Several overlapping control methods and applications have been proposed, see for example (Trudnowski and Pierre, 1992), (Bakule et al., 2006), (Hug-Glanzmann and Andersson, 2009), (Ahmadi and Aldeen, 2017).

A highway is an one-dimensional structure, where traffic flow is modelled on the basis of a tandem of sections (each about 500 m long), each of them interacting with its two adjacent sections. More specifically, the information flow in the highway traffic process points downstream in free-flow conditions; and upstream in congested conditions. The research question investigated in this paper is whether the centralized IBC-LQR may be replaced, without significant loss of efficiency, by a tandem of local sub-controllers, each dealing with a corresponding subsystem that consists of a few subsequent highway sections. Given the interactions among adjacent sections, the subsystems should be overlapping, i.e., adjacent subsystems have one or more sections in common. Such a decentralization may reduce the regulator design effort in cases of very long highways; and would certainly improve on the communication requirements and reliability of the overall control system.

This paper introduces two overlapping decentralized control schemes for IBC of lane-free automated vehicle traffic. The first approach is based on a contractible controller developed for an extended model that exploits the overlapping structure of the system. This approach allows for decomposed control design, separately for each subsystem, which enhances scalability of design and expandability of the controlled system when considering additional highway parts for control, since the additional subsystem control can be designed independently of the existing control system. The method was first introduced by Ikeda et al. (1981) and was extended by İftar and Özgüner (1990) to consider input inclusion, additionally to state inclusion. In the second approach, the discrete-time LQR problem is first transformed into a linear matrix inequalities (LMI) problem (Zečević and Šiljak (2005). The overlapping control structure used is selected, the LMI problem is solved, and the accordingly structured gain matrix is obtained, enabling a decentralized overlapping control scheme. This second approach calls for a centralized design procedure (LMI problem), but may, for this reason, lead to better control results under the same decentralized overlapping control structure, compared to the first approach.

The well-known Cell Transmission Model (CTM) (Daganzo, 1994) is used, after linearization, for controller design; and, in its full nonlinear form, for simulation testing. The next section presents some background issues and the appropriately adjusted CTM equations, while Section 3 provides the design of the proposed control schemes. Simulation investigations are discussed in Section 4 while conclusions are given in Section 5.

2 Background

Some background information on IBC modelling and centralized LQR control design, which is necessary for understanding the overlapping controller design and application, is reported in this section for completeness; see (Malekzadeh et al. 2021a; Malekzadeh et al. 2021b) for more details.

2.1 CTM for Internal Boundary Control

Lane-free traffic is not expected to give rise to structural changes of the basics of existing macroscopic traffic flow models. As also supported by results presented by Papageorgiou et al. (2021), Yanumula et al. (2021), and Malekzadeh et al. (2022), basic notions and concepts, like the conservation equation, the stationary Fundamental Diagram (FD), as well as limited-capacity bottlenecks activating congested-traffic waves, continue to characterize macroscopic traffic flow modelling in the case of lane-free automated vehicle traffic. An extended version of CTM, a first-

order dynamic traffic flow model with a triangular FD, is considered for control design (in linearized form) and for simulation testing (in full nonlinear form). Note that a triangular FD may be characterized by three parameters, e.g., the capacity q_{cap},, the critical density ρ_{cr} (at which capacity flow occurs) and the jam (maximum) density $\rho_{\max}$, see (Daganzo, 1994). The present study is focusing on the macroscopic level to test and demonstrate the unprecedented improvements enabled by IBC. The CTM is used in this context as a proxy for traffic flow modelling, under the reasonable assumption that AVs are not changing the mentioned fundamental properties of traffic, but mainly quantitative aspects (free speed, capacity, critical density values). In fact, recent, yet unpublished, CTM calibration results, using microscopic AV lane-traffic simulation data, confirm this assumption

Let us call the two opposite traffic directions, presented in Fig. 1, directions a (from left to right) and b (from right to left). The stretch is subdivided in n sections, with respective lengths L_i, $i=1,2,\ldots,n.$ The total road width (both directions) $w,$ which is assumed constant over all sections for simplicity, can be shared in real-time, independently for each section, between the two directions. As a result, each direction is assigned a corresponding road width $w_i^a=\varepsilon_i\cdot w$ and $w_i^b=(1-\varepsilon_i)\cdot w,$ where $0\le\varepsilon_i\le 1$ is the *sharing factor* per section $i=1,2,\ldots,n,$ to be specified in real-time as a control input by the internal boundary controller. The total (both directions) section capacity $q_{cap},$ as well as the total critical density ρ_{cr} and the total jam density $\rho_{\max},$ are accordingly shared between the two traffic directions a and b. Based on the derivation presented by Malekzadeh (2021a), these quantities are given by direction by

$$\begin{aligned} &q_{i,cap}^a(\varepsilon_i)=\varepsilon_i\cdot q_{cap},\ q_{i,cap}^b(\varepsilon_i)=(1-\varepsilon_i)\cdot q_{cap}\\ &\rho_{i,cr}^a(\varepsilon_i)=\varepsilon_i\cdot\rho_{cr},\ \rho_{i,cr}^b(\varepsilon_i)=(1-\varepsilon_i)\cdot\rho_{cr}\\ &\rho_{i,\max}^a(\varepsilon_i)=\varepsilon_i\cdot\rho_{\max},\ \rho_{i,\max}^b(\varepsilon_i)=(1-\varepsilon_i)\cdot\rho_{\max} \end{aligned} \tag{1}$$

For the IBC problem, the complete closure of either direction is disallowed; to this end, the assigned road width in either direction should never be less than the widest vehicles driving on the road. This requirement gives rise to stricter constraints for the sharing factors as follows

$$0<\varepsilon_{i,\min}\le\varepsilon_i\le\varepsilon_{i,\max}<1 \tag{2}$$

where $\varepsilon_{i,\min}\cdot w$ and $(1-\varepsilon_{i,\max})\cdot w$ are the minimum admissible widths to be assigned to directions a and $b,$ respectively. Another restriction to be applied to the sharing factors concerns the time-delay needed to evacuate traffic on the direction that receives a restricted width, compared to the previous control time-step. This time-delay is small in lane-free CAV traffic, where no physical barrier exists among the two traffic directions, for moderate changes of the sharing factors applied to short

sections, but needs nevertheless to be considered. Clearly, the time-delay should apply only to the traffic direction that is being widened, compared to the previous control interval; while the direction that is restricted should promptly apply the smaller width, so that CAVs therein move out of the reduced-width zone. Assume that the required time-delay is smaller than or equal to the control time interval T_c; then, the time-delay requirement is automatically fulfilled for each section i, if the sharing factors that are actually applied to the two directions, i.e. ε_i^a and ε_i^b, respectively, are calculated as follows

$$\begin{aligned} \varepsilon_i^a(k_c) &= \min\left\{\varepsilon_i(k_c), \varepsilon_i(k_c-1)\right\} \\ \varepsilon_i^b(k_c) &= \min\left\{1-\varepsilon_i(k_c), 1-\varepsilon_i(k_c-1)\right\} \end{aligned} \tag{3}$$

where $k_c = 0,1,\ldots$ is the discrete control time index. It is noted that the notation $\varepsilon_i^a(k_c)$ and $\varepsilon_i^b(k_c)$ indicates that the sharing factors are applied for the duration of the control time interval $[k_c \cdot T_c, (k_c+1)\cdot T_c)$. The above equations may be readily extended if the required time-delay is a multiple of the control time interval T_c.

Traffic flows from section 1 to section n in direction a; and from section n to section 1 in direction b (see Fig. 3 as an example). It is defined ρ_i^a, $i = 1,2,\ldots,n$, to be the traffic density (in veh/km) of section i, direction a; and ρ_i^b, $i = 1,2,\ldots,n$, the traffic density of section i, direction b. Similarly, q_i^a and q_i^b, $i = 1,2,\ldots,n$, are defined to be the mainstream exit flows (in veh/h) of section i for directions a and b, respectively. Thus, q_0^a is the feeding upstream mainstream inflow for direction a; and q_{n+1}^b is the feeding upstream mainstream inflow for direction b. Every section may have an on-ramp or an off-ramp at its upstream boundary. The on-ramp flows (if any) at section i are denoted r_i^a for direction a, and r_i^b for direction b. The off-ramp flow (if any) of section i, direction a, is calculated based on known exit rates β_i^a multiplied with the upstream-section flow, i.e. $\beta_i^a q_{i-1}^a$; and the off-ramp flow (if any) of section i, direction b, is calculated based on known exit rates β_i^b multiplied with the upstream-section flow, i.e. $\beta_i^b q_{i+1}^b$. The conservation equations for the sections of direction a are:

$$\begin{aligned} \rho_1^a(k+1) &= \rho_1^a(k) + \frac{T}{L_i}\left(q_0^a(k) - q_1^a(k)\right) \\ \rho_i^a(k+1) &= \rho_i^a(k) + \frac{T}{L_i}\left((1-\beta_i^a)q_{i-1}^a(k) - q_i^a(k) + r_i^a(k)\right),\ i = 2,3,\ldots,n \end{aligned} \tag{4}$$

where T is the model time-step, typically set equal to 5–10 s for section lengths of some 500 m, and $k = 0,1,\ldots$ is the corresponding discrete-time index of the model.

According to CTM, traffic flow is obtained as the minimum of demand and supply functions, except for the last section, where only the demand function is considered, assuming that the downstream traffic conditions are uncongested. Considering the impact of the respective sharing factors on the FDs, the flow is obtained as follows (see (Malekzadeh et al. 2021a))

$$\begin{aligned} q_i^a(k) &= \min\left\{ Q_D(\rho_i^a(k), \varepsilon_i^a(k_c)), \frac{Q_S(\rho_{i+1}^a(k), \varepsilon_{i+1}^a(k_c))}{(1-\beta_{i+1}^a)} - \lambda_r r_{i+1}^a(k) \right\},\ i = 1, 2, \ldots, n-1 \\ q_n^a(k) &= Q_D(\rho_n^a(k), \varepsilon_i^a(k_c)). \end{aligned} \tag{5}$$

The demand and supply functions are given by the following respective equations

$$\begin{aligned} Q_D(\rho, \varepsilon) &= \min\left\{ \varepsilon q_{cap} + \lambda_d q_{cap} \frac{\rho - \varepsilon\rho_{cr}}{\rho_{cr} - \rho_{\max}}, v_f \rho \right\}, \\ Q_S(\rho, \varepsilon) &= \min\left\{ \varepsilon q_{cap}, w_s(\varepsilon\rho_{\max} - \rho) \right\}, \end{aligned} \tag{6}$$

where v_f is the free speed (which is assumed equal for all sections for simplicity) and w_s is the back-wave speed. Note that, for a triangular FD, these two parameters may be deduced from q_{cap}, ρ_{cr}, and $\rho_{\max}$,; note also that the two parameters are invariant to the road width. The control time-step T_c does not need to be equal to the model time-step, but is assumed to be a multiple of T, in which case the control time index is given by $k_c = \lfloor kT/T_c \rfloor$, where $\lfloor . \rfloor$ is the integer part notation.

It is well-known that CTM does not reproduce the capacity drop phenomenon, i.e., the empirical finding that, at the head of congestion, the observed flow in real traffic is reduced, compared to the road capacity. Capacity drop is deemed to occur in conventional traffic due to bounded and differing accelerations of different vehicles (Yuan et al., 2015). Recently, CTM has been extended in a number of possible ways to enable the reproduction of capacity drop, see (Kontorinaki et al., 2017) for an overview and comparison. The presence of capacity drop in conventional freeway traffic is a major reason for infrastructure degradation and for the need of introducing traffic control measures to restore capacity (Papageorgiou et al., 2003). In contrast, in the present context of internal boundary control, the presence of capacity drop marks a secondary source of amelioration of the traffic conditions, because the potential benefits achievable via opportune capacity sharing are expected to be much higher than those resulting from capacity drop avoidance. In fact, it is unknown at the moment, if and to what extent capacity drop may occur in lane-free CAV traffic. To be able to investigate the impact of possible capacity drop, the option of introducing capacity drop has been incorporated in the above equations trough appropriate terms according to Kontorinaki et al. (2017). More specifically, this option is enabled via the parameters λ_r and λ_d in equations (5) and (6). If these parameters are set to $\lambda_r = 1$ and $\lambda_d = 0$, no capacity drop is reproduced, as typical

for CTM; if these values are set between 0 and 1, a corresponding level of capacity drop is produced by the model.

The equations for direction b are analogous to those of direction a, with few necessary index modifications. Section numbers in direction b are descending, hence

$$\begin{aligned}\rho_i^b(k+1) &= \rho_i^b(k) + \frac{T}{L_i}((1-\beta_i^b)q_{i+1}^b(k) - q_i^b(k) + r_i^b(k)),\ i = 1,2,\ldots,n-1 \\ \rho_n^b(k+1) &= \rho_n^b(k) + \frac{T}{L_i}(q_{n+1}^b(k) - q_n^b(k))\end{aligned} \tag{7}$$

and the flows are given by

$$\begin{aligned}q_1^b(k) &= Q_D(\rho_1^b(k), \varepsilon_i^b(k_c)) \\ q_i^b(k) &= \min\left\{Q_D(\rho_i^b(k), \varepsilon_i^b(k_c)), \frac{Q_S(\rho_{i-1}^b(k), \varepsilon_{i-1}^b(k_c))}{(1-\beta_{i-1}^b)} - \lambda_r r_{i-1}^b(k)\right\},\ i = 2,3,\ldots,n\end{aligned} \tag{8}$$

In conventional traffic management, traffic densities (in veh/km) characterize clearly the state of traffic, depending on their value versus the critical density: free traffic (when density is lower than critical density), critical traffic (when density is around critical density) or congested traffic (when density is higher than critical density). However, in the proposed IBC measure, the critical density for each direction and section is not constant, but a function of the sharing factor (see (1)), and is changing according to the applied control action. Therefore, the density value by itself is not sufficient, in the IBC context, to characterize the traffic situation in a section.

To address this issue, the following relations define the relative densities (dimensionless) per section and per direction. The relative density of section i and direction a or b is obtained by dividing the corresponding traffic density with the corresponding critical density, which, on its turn, depends (via (1)) on the sharing factor prevailing during the last time-step, as follows

$$\tilde{\rho}_i^a(k) = \frac{\rho_i^a(k)}{\varepsilon_i(k-1)\rho_{cr}},\ \tilde{\rho}_i^b(k) = \frac{\rho_i^b(k)}{(1-\varepsilon_i(k-1))\rho_{cr}} \tag{9}$$

The relative densities reflect clearly the state of the traffic in the IBC context. Specifically, if the relative density of a section and direction is less than 1, it reflects under-critical (free-flow) traffic conditions; if it is around 1, it reflects capacity flow; and if it is greater than 1, it reflects over-critical (congested) traffic conditions.

2.2 Centralised open-loop optimisation for Internal Boundary Control

Malekzadeh et al. (2021a) first addressed the IBC problem in lane-free traffic and demonstrated its high improvement potential by formulating and solving an open-loop optimal control problem, in

the form of a convex Quadratic Programming (QP) problem. The QP problem minimizes a physical performance criterion, the total time spent by all vehicles over a time horizon, along with some operational sub-objectives. The full CTM model is considered in the optimization problem, albeit with an appropriate transformation of the piecewise linear (triangular) FD, so as to involve only linear equality and inequality constraints and enable the usage of efficient QP solution algorithms. Availability of demands over the considered time horizon is necessary. That approach may be used within a Model Predictive Control (MPC) frame, with online demand prediction, for real-time application. In an open-loop setting, the approach delivers the maximum achievable performance, as it is based on the full CTM equations, considers all constraints and external inputs (demands) and minimizes a physical performance criterion. Therefore, in this paper, the QP approach is used as a benchmark, delivering an upper bound of achievable performance, against which other, simpler approaches may be compared.

2.3 Centralised LQR design for Internal Boundary Control

The QP approach is efficient, but simpler real-time approaches with similar efficiency, but without the need for online demand prediction, are preferable. Therefore, feedback-based Linear-Quadratic Regulators (LQR) have been developed by Malekzadeh et al. (2021b) for IBC, aiming at balancing the relative densities in the two directions; and have been demonstrated to be robust and similarly efficient as the open-loop QP solution, while avoiding the need for accurate modelling and external demand prediction.

Linearization of the CTM dynamic equations around a nominal point was presented analytically by Malekzadeh (2021b). To achieve this, the one-step retarded control input was defined as a new state variable according to $\gamma_i(k+1) = \varepsilon_i(k), \quad i = 1, 2, \ldots, n.$ Following the linearization procedure by Malekzadeh (2021b), the linearized state-space model is

$$\mathbf{x}(k+1) = \hat{\mathbf{A}}\mathbf{x}(k) + \hat{\mathbf{B}}\mathbf{u}(k) \tag{10}$$

where $\mathbf{x}(k) = [\Delta\tilde{\rho}_1^a(k), \Delta\tilde{\rho}_1^b(k), \Delta\gamma_1(k), ..., \Delta\tilde{\rho}_n^a(k), \Delta\tilde{\rho}_n^b(k), \Delta\gamma_n(k)]^T$ is the state vector and $\mathbf{u}(k) = \boldsymbol{\Delta\varepsilon}(k)$ is the control vector, whereby $\boldsymbol{\Delta\varepsilon}(k) = [\Delta\varepsilon_1(k), \ldots, \Delta\varepsilon_n(k)]^T$. Also, $\Delta(.)(k) = (.)(k) - (.)^N$, the superscript N denoting the nominal values, while it has been assumed that $\Delta(.)(k) = 0$ for all disturbances (upstream mainstream inflows, as well as the on-ramp flows, of each direction). $\hat{\mathbf{A}} \in \mathbb{R}^{3n \times 3n}$ and $\hat{\mathbf{B}} \in \mathbb{R}^{3n \times n}$ are the time-invariant state and input matrices, respectively, while $\mathbf{x} \in \mathbb{R}^{3n}$ and $\mathbf{u} \in \mathbb{R}^n$.

If the control time-step is defined as a multiple of the model time-step, i.e. $T_c = MT$, where M is an integer, then the discrete control time index is $k_c = \lfloor kT/T_c \rfloor$. Thus, the linear state-space equation may be changed as follows, in order to be based on the control time-step T_c,

$$\varphi : \mathbf{x}(k_c + 1) = \mathbf{A}\mathbf{x}(k_c) + \mathbf{B}\mathbf{u}(k_c) \tag{11}$$

where $\mathbf{A} = \hat{\mathbf{A}}^M$, and $\mathbf{B} = (\hat{\mathbf{A}}^{M-1} + \hat{\mathbf{A}}^{M-2} + ... + \mathbf{I})\hat{\mathbf{B}}$.

When employing the LQR methodology, as done by Malekzadeh (2021b), the control goal is the minimization of the quadratic criterion

$$J = \frac{1}{2}\sum_{k_c=0}^{\infty}\left[\mathbf{x}^T(k_c)\mathbf{Q}\mathbf{x}(k_c) + \mathbf{u}^T(k_c)\mathbf{R}\mathbf{u}(k_c)\right] \tag{12}$$

where $\mathbf{Q} \in \mathbb{R}^{3n\times 3n}$ is a diagonal positive semidefinite matrix and $\mathbf{R} \in \mathbb{R}^{n\times n}$ is a diagonal positive definite matrix. The first term penalizes deviations of the state variables from zero, i.e. deviations of $\tilde{\rho}_i^a(k_c)$, $\tilde{\rho}_i^b(k_c)$, $\gamma_i(k_c)$, $i = 1, 2, \ldots, n$, from their respective desired nominal values. The second term penalizes deviations of the control inputs from the nominal values.

The nominal value of relative densities on both directions is set equal to 1 (with positive, under-critical derivative), so that the controller is motivated to operate the system near capacity, which is good for traffic efficiency. In particular, due to the quadratic penalty terms, the controller tends to mitigate strong density departures from the critical density at specific sections, i.e., mitigate traffic congestion. In addition, if capacity flow is not feasible (e.g. due to lack of demand), then minimizing a sum of squares has the tendency to balance deviations from the nominal values at different sections and directions, something that is conform with the secondary operational sub-objective of balancing the margin to capacity across sections and directions. On the other hand, the nominal value for the sharing factors is set to 0.5, so as to have smooth and moderate internal boundary changes. Thus, minimization of the second term in (12) mitigates deviations of the sharing factors from 0.5 and balances these deviations in space and time, which is a secondary operational sub-objective, as unnecessarily strong internal boundary changes over space and time should be avoided.

The optimal controller minimizing the criterion (12) subject to the model (11) is given by a linear state-feedback control law of the form $\mathbf{u}(k_c) = \mathbf{K}\mathbf{x}(k_c)$, where $\mathbf{K} \in \mathbb{R}^{n\times 3n}$ is a constant gain matrix given by

$$\mathbf{K} = (\mathbf{R} + \mathbf{B}^T\mathbf{P}\mathbf{B})^{-1}\mathbf{B}^T\mathbf{P}\mathbf{A} \tag{13}$$

and $\mathbf{P}$ is a unique positive semidefinite solution of the discrete-time algebraic Riccati equation.

3 Overlapping control schemes

Summarizing from above, each highway section (of some 500 m length) has three state variables and one control input, which is the corresponding sharing factor. For very long highways, designing the centralized LQR, proposed by Malekzadeh (2021b) and outlined above, calls for the solution of an accordingly large-scale Riccati equation. More importantly, the centralized LQR requires real-time information for all the states of the system even very remote ones, to compute each control input. This requirement may be problematic for long highways due to the need to transfer data from the whole highway in order to compute each sharing factor. Lastly, the traffic situation may be quite different at different parts of a long highway; then, balancing relative densities and sharing factors over the whole highway may not be fully relevant, as it is reasonable to address this sub-objective primarily at local levels.

For the above reasons, there is an interest in developing a decentralized control scheme, which may reduce the LQR design complexity; reduce the burden of real-time data transferring; and increase the system reliability in cases of device failure. Due to strong dependencies between consecutive sections in traffic flow, developing a fully decentralized control scheme (with disjoint subsystems) may reduce the control efficiency compared to the centralized case, as was indeed confirmed in preliminary investigations. Therefore, in this study, overlapping control schemes are adopted and tested for IBC. The approaches rely on the separation of the highway in a number of subsequent subsystems (highway stretches) which are overlapping, i.e., adjacent subsystems have some sections in common; hence, adjacent subsystems share some states and some control inputs. This approach delivers overlapping decentralized controllers, where, thanks to the overlapping structure, subsystems remain partly aware about the inter-relations with adjacent subsystems. Overlapping controllers offer less communication and equipment requirements, less monitoring and maintenance effort and higher reliability versus the centralized LQR, for the price of a minor performance reduction. It is hardly possible to predict appropriate trade-offs of these features versus performance, therefore the paper investigates the issue empirically, using different overlapping structures

The control inputs of the non-overlapping sections are computed based only on local subsystem information; while control inputs in the overlapping sections use information from both adjacent subsystems. The following sections present the details of the employed overlapping control approaches. The structure of the overlapping control scheme is illustrated in Fig. 2 for a two-subsystem case with one overlapping section. The overlapping section 4 delivers real-time

measurements to both adjacent subsystem controllers; and its control input is specified with contributions from both adjacent subsystem controllers.

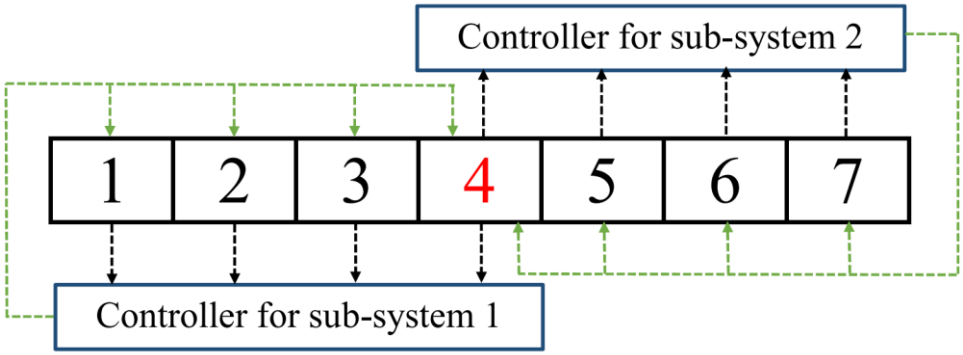

Fig. 2: A block diagram of overlapping control scheme for two subsystems.

3.1 Contractible controller design with state and input inclusion

Consider the following linear time-invariant system

$$\tilde{\varphi}:\ \tilde{\mathbf{x}}(k_c+1)=\tilde{\mathbf{A}}\tilde{\mathbf{x}}(k_c)+\tilde{\mathbf{B}}\tilde{\mathbf{u}}(k_c) \tag{14}$$

where $\tilde{\mathbf{x}}\in\mathbb{R}^{\tilde{n}}$ and $\tilde{\mathbf{u}}\in\mathbb{R}^{\tilde{m}}$. In the following, the system φ in (11) is referred to as the original system, and $\tilde{\varphi}$ is referred to as the expanded system. It is assumed that $\tilde{n}\geq 3n$ and $\tilde{m}\geq n$, as the expanded system $\tilde{\varphi}$ has typically more states and more inputs than the original system φ due to the expansion. More specifically, the goal of the expansion is to create overlapping areas that belong to both corresponding adjacent subsystems, and this leads to higher state and control dimensions for the expanded system.

The state and the input of the original system are partitioned as

$$\begin{aligned}\mathbf{x}&=(\mathbf{x}_1^T,\mathbf{x}_2^T,\ldots,\mathbf{x}_P^T),\quad \mathbf{x}_i\in\mathbb{R}^{n_i}\\ \mathbf{u}&=(\mathbf{u}_1^T,\mathbf{u}_2^T,\ldots,\mathbf{u}_P^T),\quad \mathbf{u}_i\in\mathbb{R}^{m_i}\end{aligned} \tag{15}$$

where $P\geq 3$ is the odd number of partitions (subsequent highway stretches). Here it is assumed that, for all even indexes i, $\mathbf{x}_i$ and $\mathbf{u}_i$ correspond to the overlapping parts of the state and input vectors, respectively, while for all odd indexes i, $\mathbf{x}_i$ and $\mathbf{u}_i$ correspond to the non-overlapping parts of the state and input spaces.

Now consider that the matrices $\mathbf{A}$ and $\mathbf{B}$ for the system φ are also partitioned compatibly, as follows:

$$\begin{bmatrix} \mathbf{A}_{11} & \mathbf{A}_{12} & \cdots & \mathbf{A}_{1P} \\ \mathbf{A}_{21} & \mathbf{A}_{22} & \cdots & \mathbf{A}_{2P} \\ \vdots & \vdots & \ddots & \vdots \\ \mathbf{A}_{P1} & \mathbf{A}_{P2} & \cdots & \mathbf{A}_{PP} \end{bmatrix}, \begin{bmatrix} \mathbf{B}_{11} & \mathbf{B}_{12} & \cdots & \mathbf{B}_{1P} \\ \mathbf{B}_{21} & \mathbf{B}_{22} & \cdots & \mathbf{B}_{2P} \\ \vdots & \vdots & \ddots & \vdots \\ \mathbf{B}_{P1} & \mathbf{B}_{P2} & \cdots & \mathbf{B}_{PP} \end{bmatrix}. \tag{16}$$

An expanded system $\tilde{\varphi}$ can be obtained from the original system φ, as will be explained below. If the expanded system satisfies certain conditions presented by İftar and Özgüner (1990), such an expansion is called an extension and can be leveraged in order to design the controller for the original system based on the design of a controller for the extended system. For the case of overlapping areas belonging to exactly two corresponding adjacent subsystems, as in the IBC application, the expanded system matrices $\tilde{\mathbf{A}}$ and $\tilde{\mathbf{B}}$ can be easily obtained from the original matrices $\mathbf{A}$ and $\mathbf{B}$ by simply doubling the state equations of the overlapping partitions. This expansion may be readily shown to satisfy the conditions required in (İftar and Özgüner, 1990) for an extension of the original system.

A highway stretch that is subdivided in 10 sections (see Fig. 3) is considered as an example. This system may be separated in two subsystems with a single overlapping area of two sections, i.e. based on three partitions ($P=3$) of the original system. As can be seen in Fig. 3, two subsystems with six sections each are introduced; while sections 5 and 6 are considered as an overlapping area. The two subsystems are strongly connected through the overlapping area. The matrices for the extended system with $P=3$ are obtained by doubling the state equations of the overlapping sections:

$$\tilde{\mathbf{A}} = \left[\begin{array}{cc:cc} \mathbf{A}_{11} & \mathbf{A}_{12} & 0 & \mathbf{A}_{13} \\ \mathbf{A}_{21} & \mathbf{A}_{22} & 0 & \mathbf{A}_{23} \\ \hdashline \mathbf{A}_{21} & 0 & \mathbf{A}_{22} & \mathbf{A}_{23} \\ \mathbf{A}_{31} & 0 & \mathbf{A}_{32} & \mathbf{A}_{33} \end{array}\right] \triangleq \begin{bmatrix} \tilde{\mathbf{A}}_1 & \tilde{\mathbf{A}}_{12} \\ \tilde{\mathbf{A}}_{21} & \tilde{\mathbf{A}}_2 \end{bmatrix} \tag{17}$$

$$\tilde{\mathbf{B}} = \left[\begin{array}{cc:cc} \mathbf{B}_{11} & \mathbf{B}_{12} & \mathbf{B}_{12} & \mathbf{B}_{13} \\ \mathbf{B}_{21} & \mathbf{B}_{22} & \mathbf{B}_{22} & \mathbf{B}_{23} \\ \hdashline \mathbf{B}_{21} & \mathbf{B}_{22} & \mathbf{B}_{22} & \mathbf{B}_{23} \\ \mathbf{B}_{31} & \mathbf{B}_{32} & \mathbf{B}_{32} & \mathbf{B}_{33} \end{array}\right] \triangleq \begin{bmatrix} \tilde{\mathbf{B}}_1 & \tilde{\mathbf{B}}_{12} \\ \tilde{\mathbf{B}}_{21} & \tilde{\mathbf{B}}_2 \end{bmatrix} \tag{18}$$

Note that in the specific IBC application, the non-zero coupling matrices $\tilde{\mathbf{A}}_{12}$, $\tilde{\mathbf{A}}_{21}$, $\tilde{\mathbf{B}}_{12}$ and $\tilde{\mathbf{B}}_{21}$ have most of their elements equal to zero.

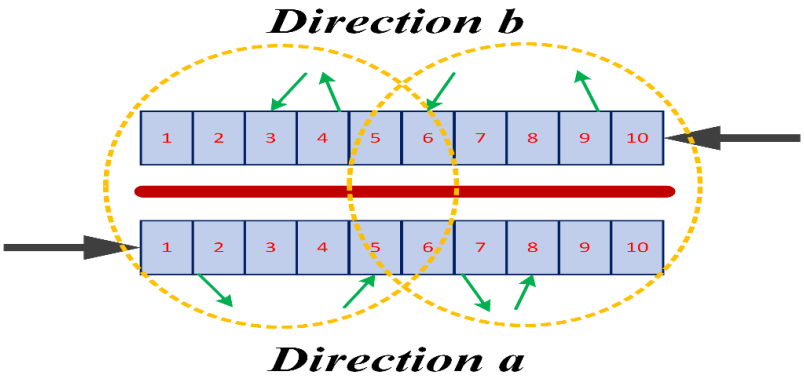

Fig. 3: A highway stretch example.

For the general case, consider $n_D = (P+1)/2$ decoupled subsystems:

$$\varphi_i^D : \tilde{\mathbf{x}}_i(k_c+1) = \tilde{\mathbf{A}}_i \tilde{\mathbf{x}}_i(k_c) + \tilde{\mathbf{B}}_i \tilde{\mathbf{u}}_i(k_c), \; i = 1, \ldots n_D \tag{19}$$

where

$$\tilde{\mathbf{A}}_1 = \begin{bmatrix} \mathbf{A}_{11} & \mathbf{A}_{12} \\ \mathbf{A}_{21} & \mathbf{A}_{22} \end{bmatrix}, \quad \tilde{\mathbf{A}}_{n_D} = \begin{bmatrix} \mathbf{A}_{(P-1)(P-1)} & \mathbf{A}_{(P-1)P} \\ \mathbf{A}_{P(P-1)} & \mathbf{A}_{PP} \end{bmatrix},$$
$$\tilde{\mathbf{A}}_i = \begin{bmatrix} \mathbf{A}_{(2i-2)(2i-2)} & \mathbf{A}_{(2i-2)(2i-1)} & \mathbf{A}_{(2i-2)(2i)} \\ \mathbf{A}_{(2i-1)(2i-2)} & \mathbf{A}_{(2i-1)(2i-1)} & \mathbf{A}_{(2i-1)(2i)} \\ \mathbf{A}_{(2i)(2i-2)} & \mathbf{A}_{(2i)(2i-1)} & \mathbf{A}_{(2i)(2i)} \end{bmatrix}, \quad i = 2, \ldots, n_D - 1 \tag{20}$$

and

$$\tilde{\mathbf{B}}_1 = \begin{bmatrix} \mathbf{B}_{11} & \mathbf{B}_{12} \\ \mathbf{B}_{21} & \mathbf{B}_{22} \end{bmatrix}, \tilde{\mathbf{B}}_{n_D} = \begin{bmatrix} \mathbf{B}_{(P-1)(P-1)} & \mathbf{B}_{(P-1)P} \\ \mathbf{B}_{P(P-1)} & \mathbf{B}_{PP} \end{bmatrix},$$
$$\tilde{\mathbf{B}}_i = \begin{bmatrix} \mathbf{B}_{(2i-2)(2i-2)} & \mathbf{B}_{(2i-2)(2i-1)} & \mathbf{B}_{(2i-2)(2i)} \\ \mathbf{B}_{(2i-1)(2i-2)} & \mathbf{B}_{(2i-1)(2i-1)} & \mathbf{B}_{(2i-1)(2i)} \\ \mathbf{B}_{(2i)(2i-2)} & \mathbf{B}_{(2i)(2i-1)} & \mathbf{B}_{(2i)(2i)} \end{bmatrix}, \quad i = 2, \ldots, n_D - 1. \tag{21}$$

The gains can be calculated for the feedback law for each decoupled subsystem $\tilde{\mathbf{u}}_i(k_c) = \tilde{\mathbf{K}}^i \tilde{\mathbf{x}}_i(k_c)$ using the LQR method for objectives similar to (12). The resulting subsystem gains $\tilde{\mathbf{K}}^i$ are partitioned as follows:

$$\tilde{\mathbf{K}}^i = \begin{bmatrix} \tilde{\mathbf{K}}^i_{11} & \tilde{\mathbf{K}}^i_{12} \\ \tilde{\mathbf{K}}^i_{21} & \tilde{\mathbf{K}}^i_{22} \end{bmatrix}, \quad i = 1, n_D$$
$$\tilde{\mathbf{K}}^i = \begin{bmatrix} \tilde{\mathbf{K}}^i_{11} & \tilde{\mathbf{K}}^i_{12} & \tilde{\mathbf{K}}^i_{13} \\ \tilde{\mathbf{K}}^i_{21} & \tilde{\mathbf{K}}^i_{22} & \tilde{\mathbf{K}}^i_{23} \\ \tilde{\mathbf{K}}^i_{31} & \tilde{\mathbf{K}}^i_{32} & \tilde{\mathbf{K}}^i_{33} \end{bmatrix}, \quad i = 2, \ldots, n_D - 1. \tag{22}$$

The overall gain for the feedback control law of the extended system $\tilde{\mathbf{u}}(k_c) = \tilde{\mathbf{K}}\tilde{\mathbf{x}}(k_c)$ is given by

$$\tilde{\mathbf{K}} = \text{blockdiag}(\tilde{\mathbf{K}}^1, \ldots, \tilde{\mathbf{K}}^{n_D}). \tag{23}$$

If $\tilde{\varphi}$ is an extension of φ, then the gain value $\mathbf{K}$ for the equivalent feedback control law of the original system, i.e. $\mathbf{u}(k_c) = \mathbf{K}\mathbf{x}(k_c)$, can be constructed using the gain value $\tilde{\mathbf{K}}$ from the feedback law of the extended system $\tilde{\mathbf{u}}(k_c) = \tilde{\mathbf{K}}\tilde{\mathbf{x}}(k_c)$ (İftar and Özgüner, 1990). For the case of the overlapping systems considered here, the gain is as follows:

$$\mathbf{K} = \begin{bmatrix} \tilde{\mathbf{K}}_{11}^1 & \tilde{\mathbf{K}}_{12}^1 & 0 & 0 & 0 & 0 & \cdots & 0 \\ \tilde{\mathbf{K}}_{21}^1 & \tilde{\mathbf{K}}_{22}^1 + \tilde{\mathbf{K}}_{11}^2 & \tilde{\mathbf{K}}_{12}^2 & \tilde{\mathbf{K}}_{13}^2 & 0 & 0 & \cdots & 0 \\ 0 & \tilde{\mathbf{K}}_{21}^2 & \tilde{\mathbf{K}}_{22}^2 & \tilde{\mathbf{K}}_{23}^2 & 0 & 0 & \cdots & 0 \\ 0 & \tilde{\mathbf{K}}_{31}^2 & \tilde{\mathbf{K}}_{32}^2 & \tilde{\mathbf{K}}_{33}^2 + \tilde{\mathbf{K}}_{11}^3 & \tilde{\mathbf{K}}_{12}^3 & \tilde{\mathbf{K}}_{13}^3 & \cdots & 0 \\ 0 & 0 & 0 & \tilde{\mathbf{K}}_{21}^3 & \tilde{\mathbf{K}}_{22}^3 & \tilde{\mathbf{K}}_{23}^3 & \cdots & 0 \\ 0 & 0 & 0 & \tilde{\mathbf{K}}_{31}^3 & \tilde{\mathbf{K}}_{32}^3 & \tilde{\mathbf{K}}_{33}^3 + \tilde{\mathbf{K}}_{11}^4 & \cdots & 0 \\ \vdots & \vdots & \vdots & \vdots & \vdots & \vdots & \ddots & \vdots \\ 0 & 0 & 0 & 0 & 0 & 0 & \ldots & \tilde{\mathbf{K}}_{22}^{n_D} \end{bmatrix} \tag{24}$$

and for the specific case of two subsystems:

$$\mathbf{K} = \begin{bmatrix} \tilde{\mathbf{K}}_{11}^1 & \tilde{\mathbf{K}}_{12}^1 & 0 \\ \tilde{\mathbf{K}}_{21}^1 & \tilde{\mathbf{K}}_{22}^1 + \tilde{\mathbf{K}}_{11}^2 & \tilde{\mathbf{K}}_{12}^2 \\ 0 & \tilde{\mathbf{K}}_{21}^2 & \tilde{\mathbf{K}}_{22}^2 \end{bmatrix}. \tag{25}$$

The approach presented above has advantages as well as some disadvantages. Traffic conditions on a long highway are usually inhomogeneous, i.e. they may be simultaneously free-flowing, critical or congested at different highway parts. In such circumstances, the mentioned balancing of relative density and sharing factor deviations from their respective nominal values may not be fully appropriate when applied to all sections of the long highway, as in the case of the centralized LQR control approach, due to strong differences in the prevailing traffic conditions. It appears more reasonable to consider subsystems with corresponding sub-objectives as done here. Additionally, this method may enhance the extendibility to new parts of a highway, as this may be done without the need for re-designing the controllers for the whole highway. On the other hand, it is evident that the decoupled, independently designed control systems cannot capture fully the dynamics of the extended system due to only partial consideration of the interconnections among subsystems. Therefore, the proposed decentralized overlapping controller (called overlapping LQR or OLQR when presenting the results) is expected to be sub-optimal compared to the centralized LQR control approach.

3.2 Overlapping control scheme using Linear Matrix Inequalities (LMIs)

Rewriting the quadratic criterion (12) yields

$$J = \frac{1}{2}\sum_{k_c=0}^{\infty}\left[\mathbf{x}^T(k_c)\mathbf{Q}\mathbf{x}(k_c) + \mathbf{u}^T(k_c)\mathbf{R}\mathbf{u}(k_c)\right]$$
$$= \frac{1}{2}\sum_{k_c=0}^{\infty}\left[(\mathbf{Q}^{1/2}\mathbf{x}(k_c))^T\mathbf{Q}^{1/2}\mathbf{x}(k_c) + (\mathbf{R}^{1/2}\mathbf{u}(k_c))^T\mathbf{R}^{1/2}\mathbf{u}(k_c)\right] \quad (26)$$

where, as already stated above, $\mathbf{Q} \in \mathbb{R}^{3n\times 3n}$ is for IBC a diagonal positive semidefinite matrix and $\mathbf{R} \in \mathbb{R}^{n\times n}$ is a diagonal positive definite matrix. Let

$$\mathbf{C} = \begin{bmatrix}\left(\frac{1}{2}\mathbf{Q}\right)^{1/2}\\ 0_{n\times 3n}\end{bmatrix}, \quad \mathbf{D} = \begin{bmatrix}0_{3n\times n}\\ \left(\frac{1}{2}\mathbf{R}\right)^{1/2}\end{bmatrix} \quad (27)$$

and $\mathbf{Z}(k_c) = \mathbf{C}\mathbf{x}(k_c) + \mathbf{D}\mathbf{u}(k_c)$. Using the above, the objective function (26) becomes

$$J = \sum_{k=0}^{\infty}\mathbf{Z}^T(k_c)\mathbf{Z}(k_c). \quad (28)$$

Assuming the use of a linear state-feedback control law

$$\mathbf{u}(k_c) = \mathbf{K}\mathbf{x}(k_c) \quad (29)$$

leads to $\mathbf{Z}(k_c) = (\mathbf{C}+\mathbf{D}\mathbf{K})\mathbf{x}(k_c)$, and (28) becomes

$$J = \sum_{k=0}^{\infty}\left[\mathbf{x}^T(k_c)(\mathbf{C}+\mathbf{D}\mathbf{K})^T(\mathbf{C}+\mathbf{D}\mathbf{K})\mathbf{x}(k_c)\right]. \quad (30)$$

Using the trace operator $\mathbf{Tr}(.)$, (30) becomes

$$J = \sum_{k=0}^{\infty}\mathbf{Tr}\left((\mathbf{C}+\mathbf{D}\mathbf{K})\mathbf{x}(k_c)\mathbf{x}^T(k_c)(\mathbf{C}+\mathbf{D}\mathbf{K})^T\right) = \mathbf{Tr}\left((\mathbf{C}+\mathbf{D}\mathbf{K})\mathbf{P}(\mathbf{C}+\mathbf{D}\mathbf{K})^T\right) \quad (31)$$

where $\mathbf{P} = \sum_{k=0}^{\infty}\mathbf{x}(k_c)\mathbf{x}^T(k_c)$ is a symmetric positive definite matrix satisfying the following Lyapunov equation (Datta, 2004) for the linear state-space model (11) after using the feedback law (29)

$$\mathbf{P} - (\mathbf{A}+\mathbf{B}\mathbf{K})\mathbf{P}(\mathbf{A}+\mathbf{B}\mathbf{K})^T - \mathbf{x}_0\mathbf{x}_0^T = \mathbf{0} \quad (32)$$

with $\mathbf{x}_0 = \mathbf{x}(0)$. Then, defining the parameter $\gamma \in (0,1)$, the following is true

$$\mathbf{P} - (\mathbf{A}+\mathbf{B}\mathbf{K})\mathbf{P}(\mathbf{A}+\mathbf{B}\mathbf{K})^T - \gamma^2\mathbf{x}_0\mathbf{x}_0^T > \mathbf{0}. \quad (33)$$

Considering a matrix $\mathbf{F} \in \mathbb{R}^{n\times 3n}$ given by $\mathbf{F} = \mathbf{K}\mathbf{P}$, the objective function (31) becomes

$$J = \mathbf{Tr}\left((\mathbf{C}+\mathbf{D}\mathbf{F}\mathbf{P}^{-1})\mathbf{P}(\mathbf{C}+\mathbf{D}\mathbf{F}\mathbf{P}^{-1})^T\right) = \mathbf{Tr}\left((\mathbf{C}\mathbf{P}+\mathbf{D}\mathbf{F})\mathbf{P}^{-1}(\mathbf{C}\mathbf{P}+\mathbf{D}\mathbf{F})^T\right) \quad (34)$$

and (33) becomes,

$$\mathbf{P} - (\mathbf{A}\mathbf{P}+\mathbf{B}\mathbf{F})\mathbf{P}^{-1}(\mathbf{A}\mathbf{P}+\mathbf{B}\mathbf{F})^T - \gamma^2\mathbf{x}_0\mathbf{x}_0^T > \mathbf{0}. \quad (35)$$

Using the Schur complement lemma (Van Antwerp and Braatz, 2000) for an auxiliary variable $\mathbf{W} > (\mathbf{CP}+\mathbf{DF})\mathbf{P}^{-1}(\mathbf{CP}+\mathbf{DF})^T$ and for (35), the following optimization problem can be formulated

$$\begin{aligned} &\min \mathbf{Tr}(\mathbf{W}) \\ &\text{s.t.} \\ &\begin{bmatrix} \mathbf{W} & \mathbf{CP}+\mathbf{DF} \\ (\mathbf{CP}+\mathbf{DF})^T & \mathbf{P} \end{bmatrix} > \mathbf{0} \\ &\begin{bmatrix} \mathbf{P} & \mathbf{AP}+\mathbf{BF} & \gamma \mathbf{x}_0 \\ (\mathbf{AP}+\mathbf{BF})^T & \mathbf{P} & 0 \\ \gamma \mathbf{x}_0^T & 0 & \mathbf{I} \end{bmatrix} > \mathbf{0} \end{aligned} \tag{36}$$

The discrete-time LQR problem has now been transformed into an LMI problem that can be solved using infeasible path-following algorithms for solving standard semidefinite programs (Toh et al., 1999) in order to get the optimal matrices $\mathbf{F}$ and $\mathbf{P}$. The difference compared to the discrete-time LQR problem is that the structure of the gain matrix $\mathbf{K}$ can be pre-specified, before solving the LMI problem, by specifying the structure of the matrices $\mathbf{F}$ and $\mathbf{P}$. Thus, the design procedure remains a centralized one, but it delivers an overlapping decentralized control scheme for IBC of lane-free automated vehicle traffic. The overlapping control structure used can be selected appropriately for the control system and the physical system at hand, something that may call for experimentation with different possible overlapping control structures.

As an example, in the case depicted in Fig. 3, where two subsystems with a single overlapping area of two sections (sections 5 and 6) are inter-connected, the structure of the gain matrix $\mathbf{K}$ needed is the following:

$$\mathbf{K}_{10\times 30} = \begin{bmatrix} \mathbf{K}^1_{4\times 18} & \mathbf{0} \\ \hline \mathbf{K}^{1,2}_{2\times 30} & \\ \hline \mathbf{0} & \mathbf{K}^2_{4\times 18} \end{bmatrix}. \tag{37}$$

Consequently, the matrices $\mathbf{F}$ and $\mathbf{P}$ can be selected to have the following structure:

$$\mathbf{F}_{10\times 30} = \begin{bmatrix} \mathbf{F}^1_{4\times 18} & \mathbf{0} \\ \hline \mathbf{F}^{1,2}_{2\times 30} & \\ \hline \mathbf{0} & \mathbf{F}^2_{4\times 18} \end{bmatrix}, \ \mathbf{P} = \begin{bmatrix} P_1 & 0 & \dots & \dots & 0 \\ 0 & P_2 & 0 & \dots & 0 \\ 0 & \ddots & \ddots & \ddots & \vdots \\ \vdots & \ddots & \ddots & \ddots & 0 \\ 0 & \cdots & 0 & 0 & P_{30} \end{bmatrix}. \tag{38}$$

The LMI approach results in an overlapping decentralized control scheme, i.e. some of the gain matrix elements have been set equal to zero (see e.g. (37)) and, as a result, the optimal value of the objective function in (36) will be at best equal to the optimal value of the objective function (12) for

the original centralized LQR problem. Nevertheless, the whole system dynamics have been considered in the design procedure, as opposed to the case of the overlapping control design procedure presented in Section 3.1. Therefore, this strategy may lead to better performance in case of complicated scenarios with stronger interconnections.

4 Simulation investigations

4.1 Simulation set-up

The performance of the proposed overlapping control schemes is investigated using the large bi-directional highway stretch depicted in Fig. 4. The considered highway stretch has a length of 20 km and is subdivided in 40 sections of 0.5 km each. There are two aspects to be considered when selecting the length of a section. First, sections are used for modelling within the discrete CTM, where the considered length of 0.5 km is appropriate, see (Kontorinaki et al., 2017). Second, the sections are used for IBC, to determine the range of each sharing factor. For the latter, too long cells would reduce the flexibility of IBC; while too short cells would call for frequent vehicle maneuvering due to frequent road width changing. Given these, the employed cell length of 0.5 km is deemed appropriate, although other cell lengths in this order may also be employed, depending on the road infrastructure and the typical traffic conditions.

The considered highway contains eight on-ramps and off-ramps (Fig. 4) in each direction, which create realistically inhomogeneous traffic conditions in space and time. The modelling time-step, T, is set to 10 s, and the considered time horizon is 1 h. While a linearization of CTM was used for the controller design, the full nonlinear extended CTM is used to represent the emulated ground truth in this section.

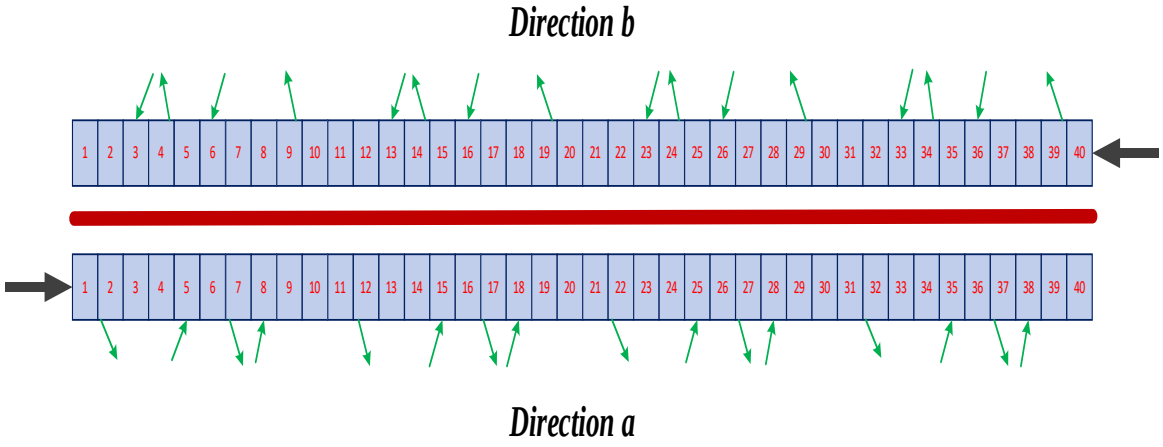

Fig. 4: The considered highway stretch.

The model parameters used in the simulation are $v_f = 100\,\text{km/h}$ and $w_s = 12\,\text{km/h}$; while the total cross-road capacity to be shared among the two directions is $q_{cap} = 12{,}000\,\text{veh/h}$. Based on the above and the triangular FD, $\rho_{cr} = 120\,\text{veh/km}$ and $\rho_{\max} = 1120\,\text{veh/km}$ can be calculated. The parameter values used to enable capacity drop are $\lambda_r = 0.7$ and $\lambda_d = 0.4$. The exit rates for all the off-ramps are set equal to 0.1.

The mainstream and on-ramp demand flows per direction are presented in Fig. 5 including two demand scenarios. The uncongested scenario causes congestion in the no-control case, but, which, by activation of the IBC, can be dissolved entirely. In the congested scenario, the no-control congestion can be mitigated by application of IBC, but cannot be utterly dissolved due to stronger overlapping between the two mainstream demands. In such cases, smart and flexible capacity sharing via IBC is still efficient, but not sufficient to utterly suppress traffic congestion. The on-ramp demands are assumed equal for all on-ramps of both directions and scenarios, as depicted in Fig. 5. It should be noted that interconnections in traffic flow are due to two main effects (Ferrara et al., 2018): (i) In free-flowing traffic, upstream traffic states (flow) influence downstream states; (ii) In congested traffic, downstream traffic states (mounting congestion tail) influence upstream states. Thus, in our considered scenarios, both effects are included to test the performance of the overlapping strategies under various levels of both mentioned effects.

As performance metrics for comparison of different approaches, two criteria are considered: (i) the Total Time Spent (TTS) by all vehicles in the highway; and (ii) the Total Delay (TD), which is the total time spent by all vehicles in excess of what would be needed if they would drive at free speed. Both metrics are expressed in (veh·h) and may be readily computed based on the macroscopic variables of the simulation model, see (Papageorgiou, et al. 2003).

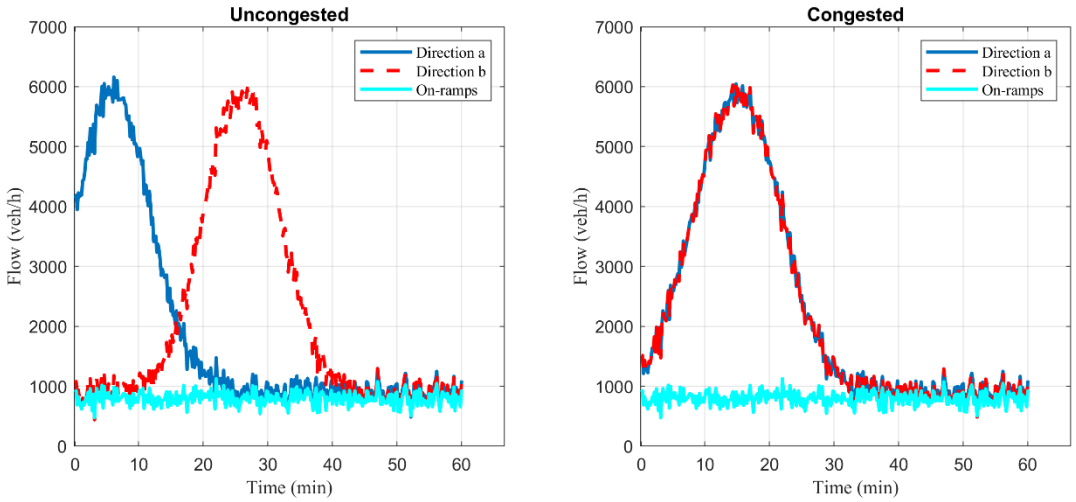

Fig. 5: Demand flows per direction and on-ramps for the uncongested scenario (left) and the congested scenario (right).

4.2 Uncongested scenario

4.2.1 No-control case

When no IBC is applied, the total width of the highway stretch is equally shared by the two directions, i.e. the sharing factors ε_i are constant and equal to 0.5 for all sections. Feeding the demand profiles, presented in Fig. 5 for the uncongested scenario, to the nonlinear CTM model with $\varepsilon_i = 0.5$, the simulation results for the no-control case are obtained. Figure 6 displays the corresponding spatio-temporal evolution of the relative density defined in (9). According to the definition, relative density values lower than 1 refer to uncongested traffic; while values higher than 1 refer to congested traffic; when the relative density equals 1, and the downstream section is uncongested, the corresponding section is at capacity flow.

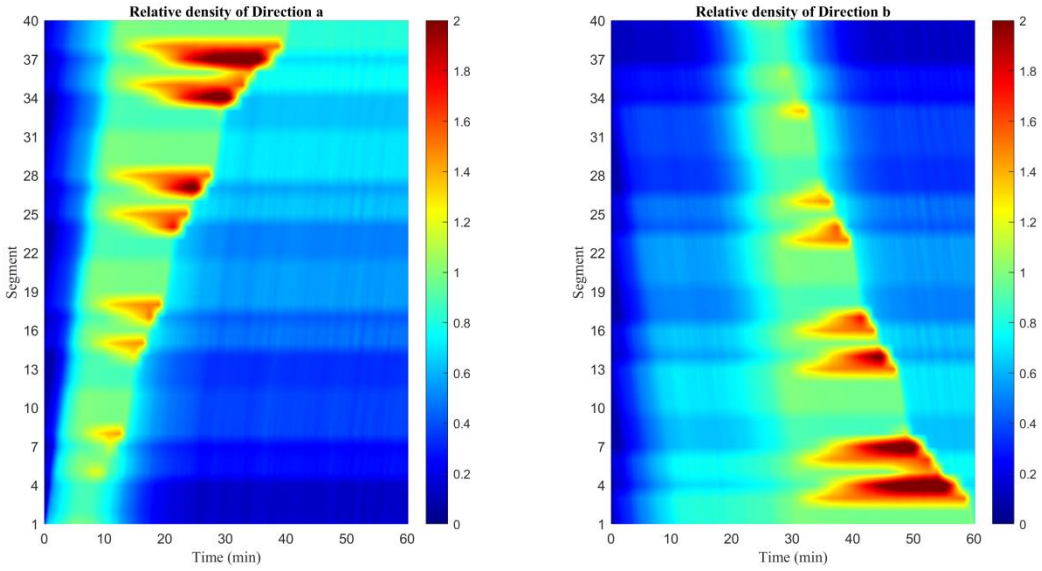

Fig. 6: Uncongested scenario: Relative density for the two directions in the no-control case.

Figure 6 shows that several congestions are created on both directions due to the high mainstream demand, in combination with the ramp inflows. As can be seen, the congestion phenomena appear around the on-ramp merge segments and, as moving downstream on each direction, the phenomena last more and cover longer areas of the highway stretch. The TTS as well as the TD performance metrics for this case are reported in Table 1.

4.2.2 Control case

To compare the performance of the proposed overlapping control schemes with previously developed methods, two centralized control schemes are considered first. The first is the QP approach (Malekzadeh et al., 2021a) and the second is the LQR approach (Malekzadeh et al., 2021b), which were outlined in Section 3.

The nominal values for linearization that is necessary for the LQR case are $q_0^a\big|_N = q_{40}^b\big|_N = 5000$ veh/h, $r_i^a\big|_N = 1000$ veh/h, $i = 5,8,15,18,25,28,35,38$, $r_i^b\big|_N = 1000$ veh/h, $i = 3,6,13,16,23,26,33,36$, $\tilde{\rho}_i^a\big|_N = \tilde{\rho}_i^b\big|_N = 1$ and $\varepsilon_i\big|_N = 0.5,\ i = 1,2,\ldots,40.$ The control time-step, T_c, is set to 60 s, hence $M = 6.$ The weighing matrices used in the objective function are selected to be $\mathbf{Q} = \mathrm{diag}(\mathbf{S}_1, \mathbf{S}_2, \ldots, \mathbf{S}_n)$ where $\mathbf{S} = [\mathbf{I}_2, \mathbf{0}_{2\times 1}; \mathbf{0}_{1\times 3}]$, $\mathbf{R} = 10^{-1}\mathbf{I}_{n\times n}$. The upper and lower bounds for the sharing factors, used to avoid utter blocking of any of the two directions, are equal for all sections $i = 1,2,\ldots,40$ and are given the values $\varepsilon_{i,\min} = 0.16$ and $\varepsilon_{i,\max} = 0.84.$ These values are used to truncate the LQR outcome.

The simulation results applying QP and LQR for the considered highway are depicted in Fig. 7. As can be seen, congestion is utterly avoided by employing open-loop QP, and the results obtained via LQR are close to that optimal solution. Table 1 figures demonstrate the effectiveness of these strategies in terms of the TTS and TD performance metrics. Note that the TD index is virtually nullified, i.e. any delays caused by traffic congestion are almost fully rejected by IBC. It is worth mentioning that in the QP problem, the smoothed versions of the demand profiles are considered as the predicted demand required by the method; while the simulations delivering the reported performance values are performed using CTM with noisy demands, as presented in Fig. 5. This is why the achieved TD improvement using the QP approach is slightly lower than 100% in this uncongested scenario.

Table 1. Uncongested scenario: TTS and TD values with related improvement (%) over the no-control case for different scenarios.

	TTS (veh·h)		**TD (veh·h)**	
No-control	1553		110.8	
Centralized	**QP**	**LQR**	**QP**	**LQR**
	1446 (6.8%)	1447 (6.8%)	3.6 (97%)	4.7 (96%)

The IBC action, while achieving the remarkable reported results, can be better understood in Fig. 8. The figure depicts flow-versus-time windows for nine selected sections, where time extends over the time-horizon of the scenario. The height of each window equals the total road capacity that must be shared among the two directions at each section. The lower displayed curve (blue) is the projected demand in direction a for each section; and the upper curve (red), starting from the upper window edge, is the projected demand in direction b. Projected demand is the flow expected in those sections in case of sufficiently high capacities to accommodate all the demands. The fact that these two curves do not intersect in the presented (and in any other) section(s), indicates that flexible capacity sharing may be applied, so as to avoid any congestion forming in either direction. Furthermore, the black line at 6000 veh/h indicates the capacity of each direction in the no-control case. Evidently, when the blue or red curve exceeds the black line, it means that the flow is higher than the capacity and a congestion is expected in the corresponding section, direction and time. The green line indicates a trajectory of capacity sharing (resulting from the corresponding sharing factor), here produced by the centralized LQR approach, which is accommodated among the blue and red curves, without ever crossing either of them. Such a sharing factor trajectory may be enabled via IBC to avoid (in this demand scenario) the otherwise unavoidable congestion. However,

this analysis also reveals that it is possible, for other demand scenarios, that IBC cannot utterly avoid the congestion, like in the next scenario, where the blue and red lines intersect; hence there is no possibility for the capacity sharing curve to separate them. In such cases, IBC will be mitigating the congestion at an extent that depends on the specific demand scenario.

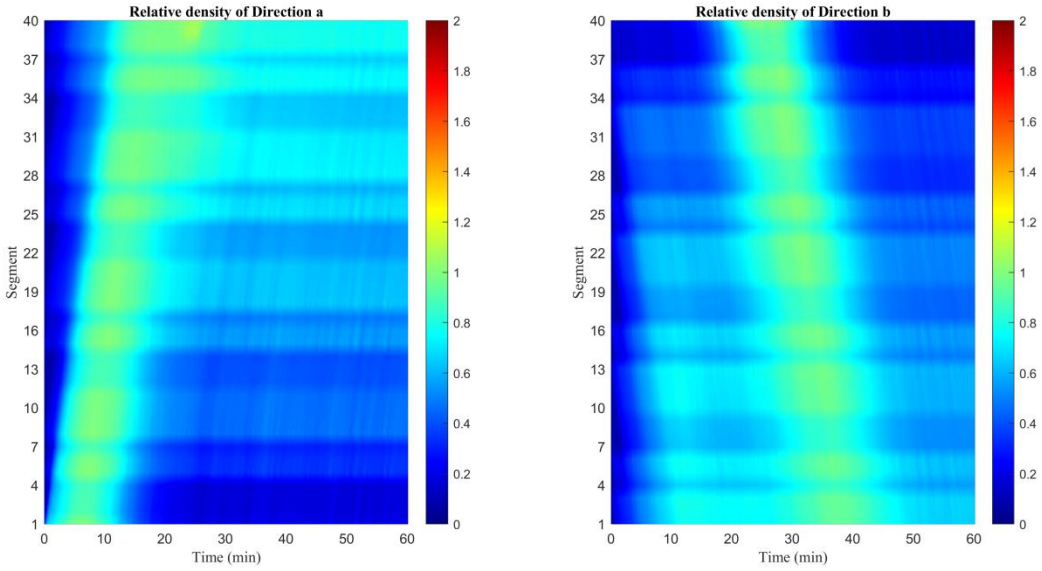

(a)

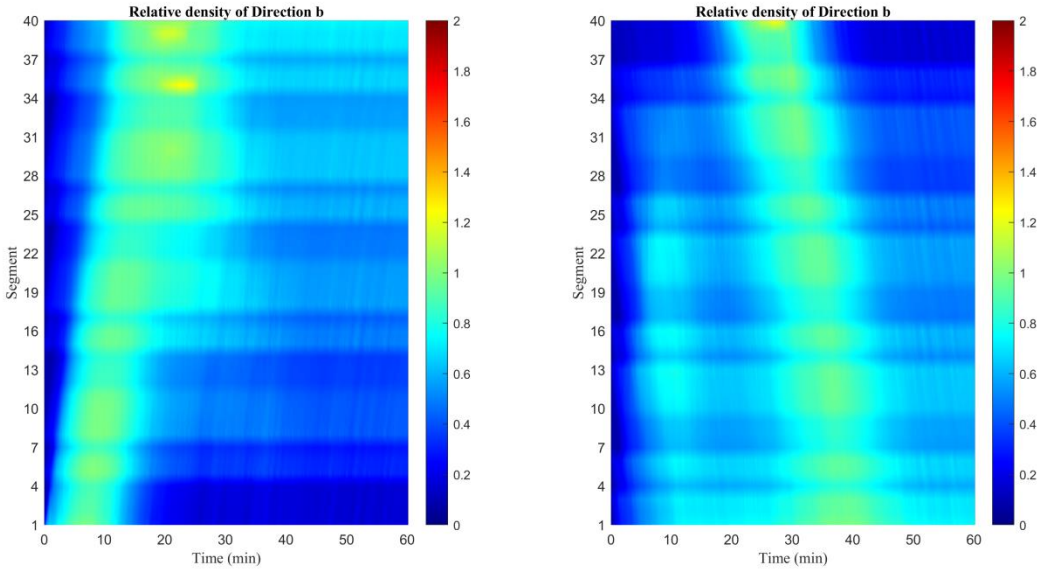

(b)

Fig. 7: Uncongested scenario: Relative density for the two directions in the centralized control cases: (a) QP; (b) LQR

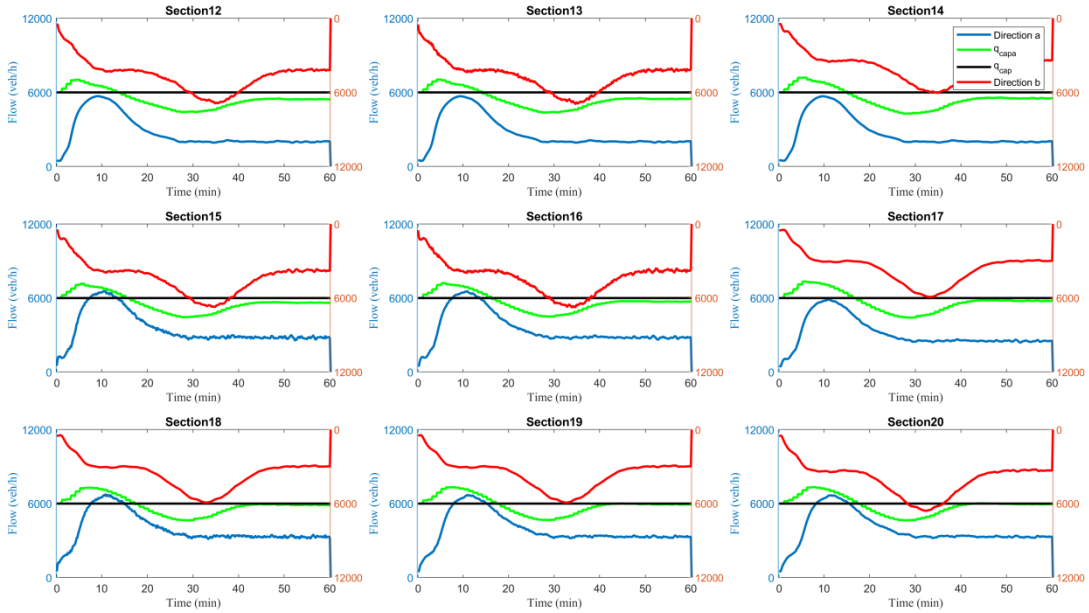

Fig. 8: Demand-supply analysis for the uncongested scenario applying centralized LQR.

In the following, the overlapping control approaches will be applied. The main issue that one must consider before applying these approaches is the arrangement of the subsystems. There are many different possibilities to choose from; the arrangement may depend on the position of the on-ramps and off-ramps, it may be symmetric or not, and may include different numbers of overlapping sections. In order to investigate some combinations, a number of different schemes with three, four or five subsystems are considered, while for each scheme the number of overlapping sections ranges from one to three. First, the highway stretch is partitioned into $P = 2n_S - 1$ partitions, where n_S is the number of subsystems considered. The partitions with an even index form the overlapping areas, while the partitions with an odd index form the non-overlapping areas. The employed overlapping control methods enable a variety of possible overlapping structures, and this calls for empirical investigations to test the performance of different such structures under realistic traffic conditions. Tables 2, 3 and 4 present the different schemes considered and the corresponding partitions. As an example, Scheme 1-2 has 5 partitions that form 3 subsystems and 2 overlapping areas composed of 2 sections each. The first subsystem includes section 1 to 14; the second subsystem includes sections 13 to 28; and the third subsystem includes sections 27 to 40.

Table 2. Distribution of sections per partition for schemes with three subsystems.

	Partitions				
	1	2	3	4	5
Scheme 1-1	1-13	14	15-26	27	28-40

Scheme 1-2	1-12	13-14	15-26	27-28	29-40
Scheme 1-3	1-11	12-14	15-25	26-28	29-40

Table 3. Distribution of sections per partition for schemes with four subsystems.

	Partitions						
	1	2	3	4	5	6	7
Scheme 2-1	1-9	10	11-19	20	21-29	30	31-40
Scheme 2-2	1-9	10-11	12-19	20-21	22-29	30-31	32-40
Scheme 2-3	1-8	9-11	12-19	20-22	23-29	30-32	33-40

Table 4. Distribution of sections per partition for schemes with five subsystems.

	Partitions								
	1	2	3	4	5	6	7	8	9
Scheme 3-1	1-7	8	9-15	16	17-23	24	25-31	32	33-40
Scheme 3-2	1-7	8-9	10-15	16-17	18-23	24-25	26-31	32-33	34-40
Scheme 3-3	1-6	7-9	10-14	15-17	18-22	23-25	26-30	31-33	34-40

The TTS and TD values related to the aforementioned schemes are presented in Table 5 for the uncongested scenario. Both approaches perform very well under all examined partitions, with the LMI approach achieving TTS and TD values closer to the centralized approaches. The results indicate that the control performance in this demand scenario is not related to the number of subsystems considered. In contrast, for all subsystem cases, the control performance is getting better when the overlapping areas include more than one section, something that underlines the necessity of considering the interconnections among subsystems for more pertinent control. As an example, the results related to scheme (2-2) for the decentralized case are depicted in Fig. 9. When compared with the results presented in Fig. 7, it can be observed that the relative density heat plots are similar as also expected from the similar efficiency improvement.

Table 5. Uncongested scenario: TTS and TD values with related improvement (%) over the no-control case for different scenarios.

	TTS (veh·h)		**TD (veh·h)**	
Decentralized	**LMI**	**OLQR**	**LMI**	**OLQR**
Scheme 1-1	1450 (6.7%)	1461 (5.9%)	7.7 (93.1%)	18.4 (83.4%)
Scheme 1-2	1448 (6.8%)	1457 (6.2%)	6.0 (94.6%)	15.3 (86.2%)
Scheme 1-3	1448 (6.8%)	1453 (6.5%)	6.3 (94.3%)	11.2 (89.9%)
Scheme 2-1	1451 (6.6%)	1452 (6.5%)	8.8 (92.1%)	9.4 (91.5%)
Scheme 2-2	1449 (6.7%)	1450 (6.7%)	6.6 (94.0%)	8.0 (92.8%)
Scheme 2-3	1448 (6.8%)	1450 (6.7%)	6.3 (94.3%)	8.0 (92.8%)
Scheme 3-1	1457 (6.2%)	1460 (6.0%)	14.5 (86.9%)	18.1 (83.7%)
Scheme 3-2	1453 (6.5%)	1457 (6.2%)	10.9 (90.2%)	14.8 (86.6%)

Scheme 3-3	1450 (6.7%)	1453 (6.5%)	7.4 (93.3%)	11.3 (89.8%)

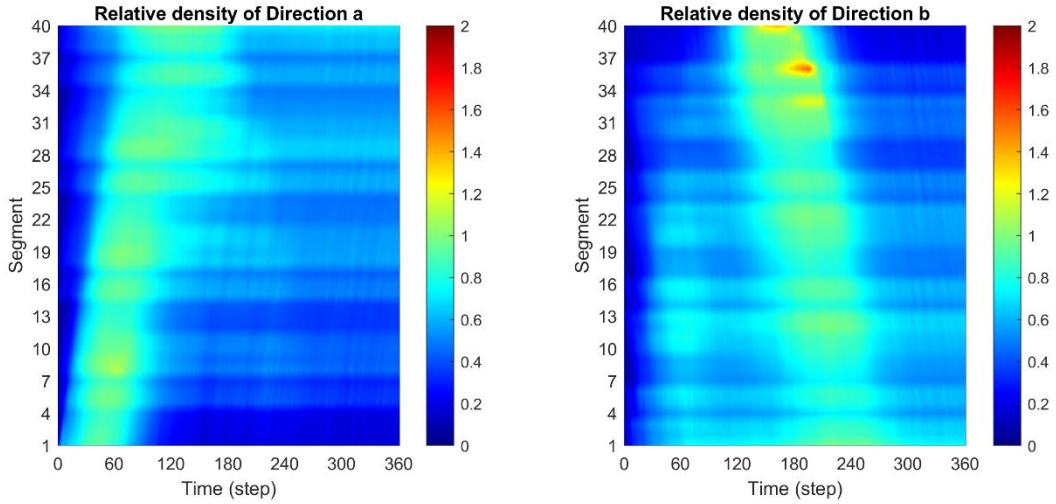

(a)

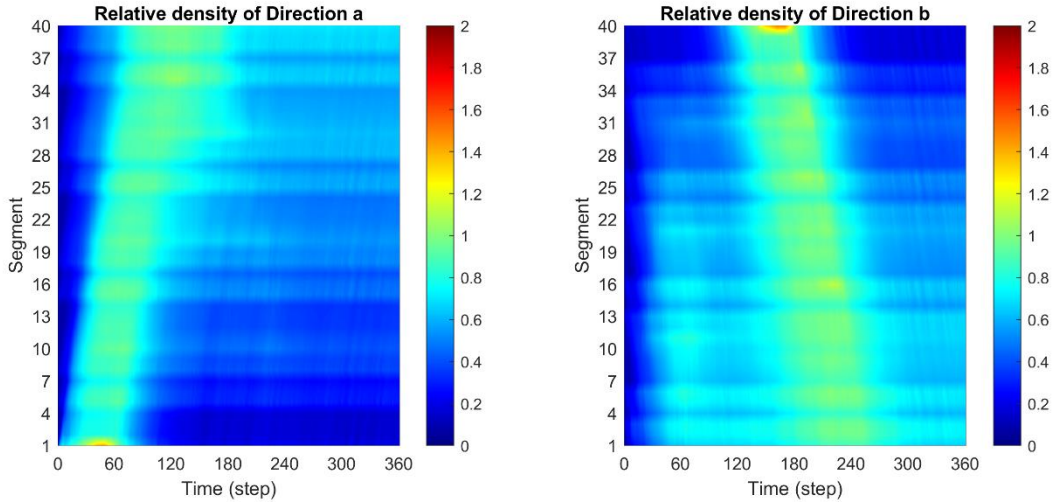

(b)

Fig. 9: Uncongested scenario: Relative density for the two directions in the decentralized control (scheme 2-2) cases: (a) LMI; (b) OLQR

4.3 Congested scenario

4.3.1 No-control case

Using the demand profiles, presented in Fig. 5 for the congested scenario, to feed the nonlinear CTM model with $\varepsilon_i = 0.5,$ the simulation results for the no-control case are obtained. Essentially,

all external flows are similar to those in the uncongested scenario, with the notable difference that the two mainstream demand profiles have been shifted so that they completely overlap with each other in time. This gives rise to strong flows on both directions at similar times, which implies limited opportunities for IBC and, indeed, capacity problems even in presence of IBC.

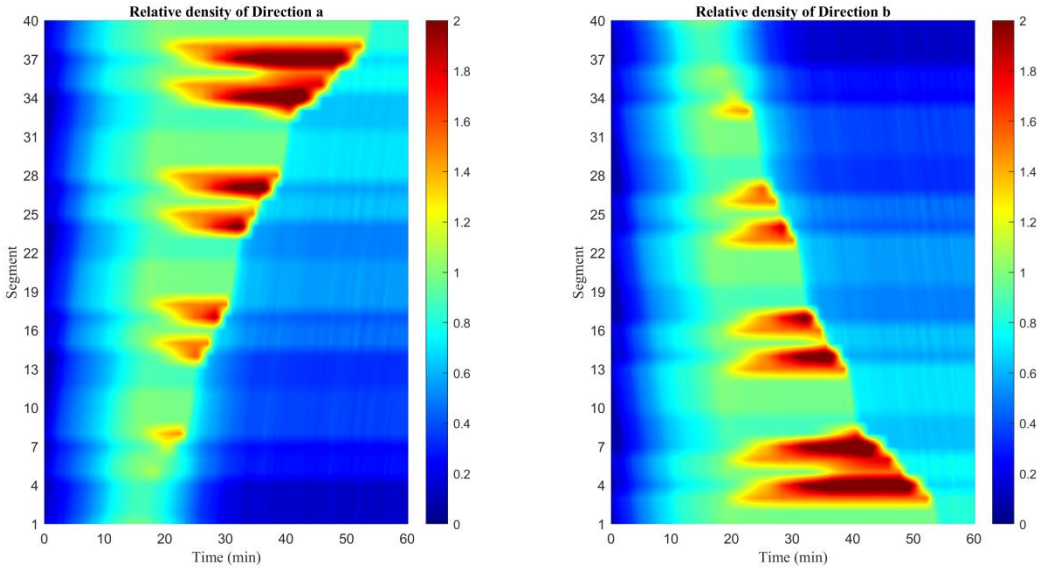

Fig. 10: Congested scenario: Relative density for the two directions in the no-control case.

Figure 10 shows that congestion areas are created on both directions due to the increased mainstream demand, in combination with the ramp inflows. As in the case of the uncongested scenario considered in Section 4.2.1, the congestion phenomena appear around the on-ramp merge segments, and, as moving further downstream on each direction, the phenomena last longer and cover longer areas of the highway stretch. The main difference here is that the phenomena are shifted in time due to the corresponding shift that has been applied to the demand profiles. The Total Time Spent (TTS) in the system as well as the Total Delay (TD) for this case are reported in Table 6.

4.3.2 Control case

The simulation results applying the centralized open-loop QP and LQR strategies for the considered highway are depicted in Fig. 11. As can be seen, congestion cannot be avoided completely with IBC, but it is strongly mitigated via flexible internal boundary moving by the control strategies. Table 6 figures demonstrate the effectiveness of these strategies with respect to TTS and TD values. The results obtained via the centralized LQR approach are, also for this scenario, very close to the

open-loop optimal solution. Notice the remarkable reduction of the TD metric, despite the challenging demand scenario with two simultaneous strong mainstream demands.

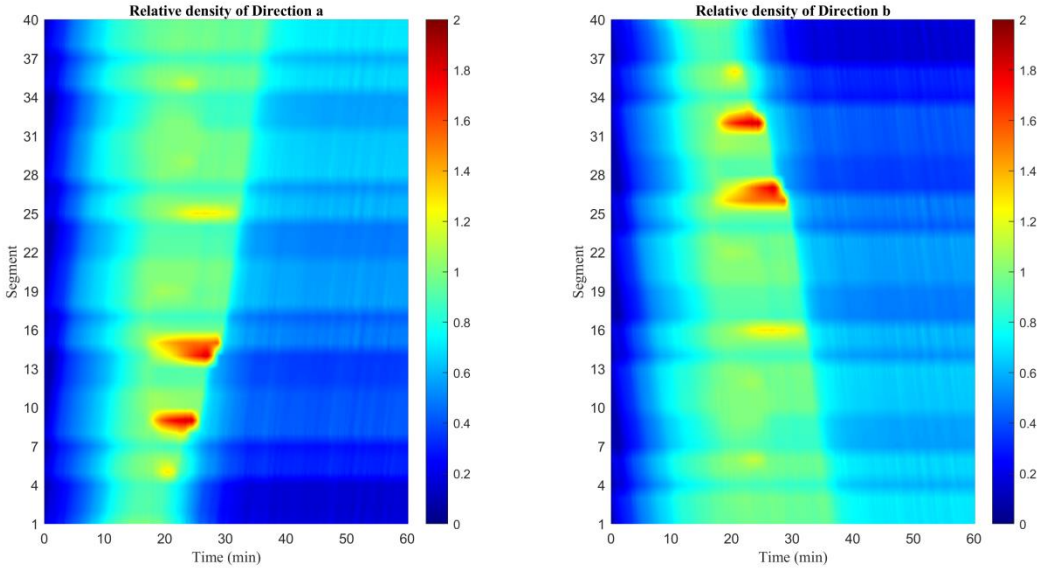

(a)

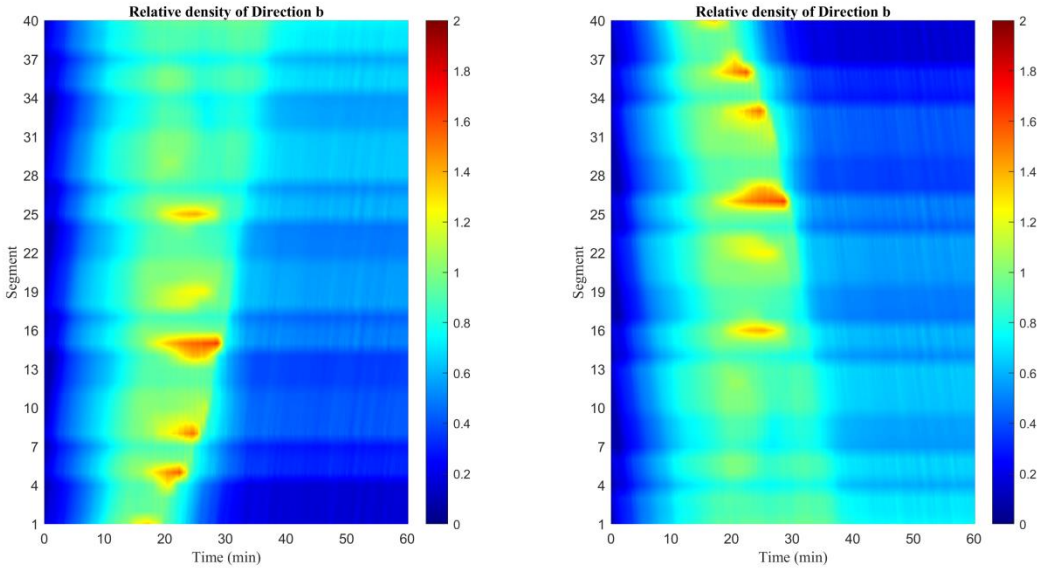

(b)

Fig. 9: Congested scenario: Relative density for the two directions in the centralized control case: (a) QP; (b) LQR

The overlapping control approaches are applied next for all the different schemes presented in Tables 2, 3 and 4. Table 6 includes the corresponding TTS and TD values for the congested scenario. Both approaches perform very well, with the LMI approach achieving TTS and TD values

closer to the centralized approaches. In this scenario, more performance variations are observed, particularly for the OLQR approach, but no consistent relation of the control performance to the number of subsystems considered or to the number of sections in the overlapping areas can be deduced.

Table 6. Congested scenario: TTS and TD values with related improvement (%) over the no-control case for different scenarios.

	TTS (veh·h)		**TD (veh·h)**	
No-control	1681		173.2	
Centralized	**QP**	**LQR**	**QP**	**LQR**
	1536 (8.7%)	1537(8.6%)	27.9 (83.9%)	29.4 (83.0%)
Decentralized	**LMI**	**OLQR**	**LMI**	**OLQR**
Scheme 1-1	1546 (8.1%)	1565 (6.9%)	37.8 (78.2%)	56.8 (67.2%)
Scheme 1-2	1542 (8.3%)	1579 (6.1%)	34.1 (80.3%)	70.9 (59.1%)
Scheme 1-3	1547 (8.0%)	1621 (3.6%)	39.0 (77.5%)	113.2 (34.6%)
Scheme 2-1	1540 (8.4%)	1587 (5.6%)	32.2 (81.4%)	78.7 (54.6%)
Scheme 2-2	1540 (8.4%)	1568 (6.8%)	32.5 (81.2%)	59.6 (65.6%)
Scheme 2-3	1541 (8.4%)	1569 (6.7%)	33.3 (80.8%)	61.3 (64.6%)
Scheme 3-1	1542 (8.3%)	1606 (4.5%)	33.9 (80.4%)	97.8 (43.5%)
Scheme 3-2	1542 (8.3%)	1614 (4.0%)	34.2 (80.3%)	107.8 (37.8%)
Scheme 3-3	1543 (8.2%)	1614 (4.0%)	34.7 (80.0%)	105.7 (39.0%)

As an example, the results related to scheme (2-2) for the decentralized control are depicted in Fig. 12. When compared with the results presented in Fig. 11, it can be observed that the relative density heat plots are quite similar, with the congestion phenomena appearing at nearby locations.

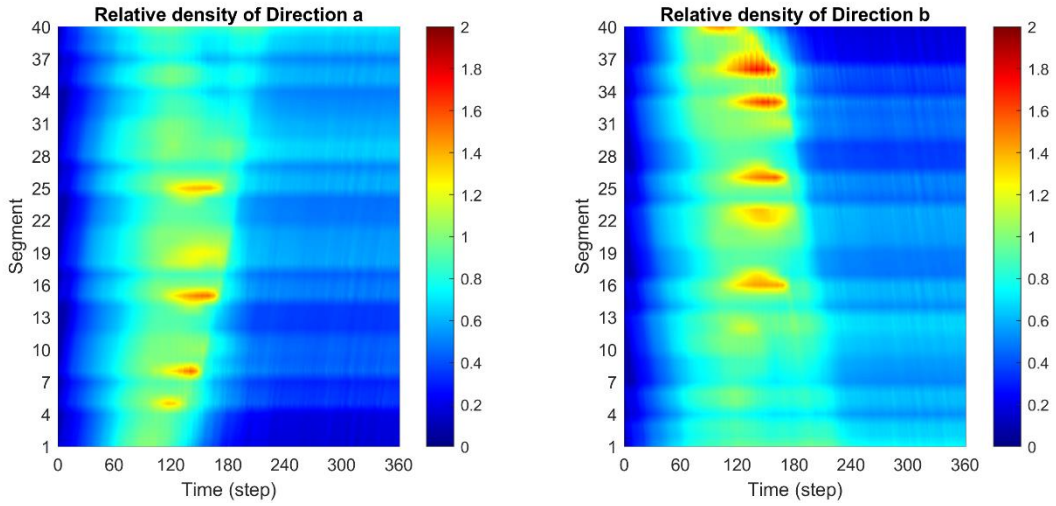

(a)

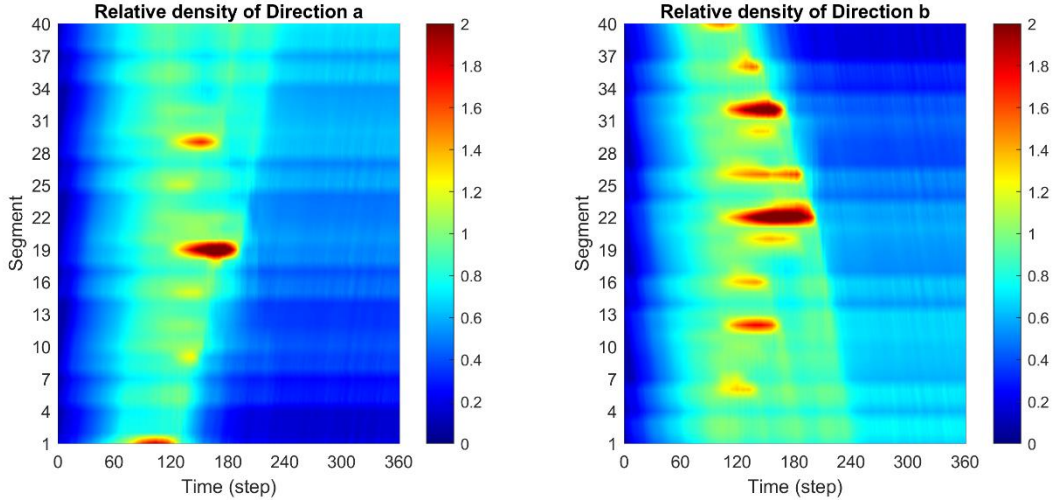

(b)

Fig. 12: Congested scenario: Relative density for the two directions in the decentralized control (scheme 2-2) cases: (a) LMI; (b) OLQR

5 Conclusions

The concept of internal boundary control, introduced by Malekzadeh et al. (2021a), has been revisited in this study by use of different feedback control approaches with an overlapping structure for a sizable highway system. According to the IBC concept, the total road width and capacity are shared in each section in real-time among the two directions of the road in response to the prevailing traffic conditions. As in previous studies, the well-known CTM, extended to include the capacity drop and appropriately adjusted to introduce the effect of the sharing factors, has been utilized (in linearized form) for the development of the overlapping decentralized regulators for the IBC problem, as well as (in full nonlinear form) for simulation testing and comparison. Two overlapping decentralized control design methods were adopted:

(i) a contractible controller with state and input inclusion developed for an extended system (İftar and Özgüner, 1990) and

(ii) a linear matrix inequalities approach (Zečević and Šiljak, 2005).

Approach (i) may be designed separately for each considered subsystem, which is favorable for scalability and extendibility in cases of long highways. In contrast, approach (ii) calls for centralized design based on a pre-selected control structure. Both overlapping regulator schemes reduce the communication, monitoring and maintainance requirements and increase control system reliability in cases of device failures, which is beneficial in case of long highways.

Simulation investigations first demonstrate the adequacy of previously developed centralized IBC approaches in sizable highway scenarios. Regarding the novel overlapping decentralized control schemes, it was found that, for the case of the uncongested demand scenario (where congestion is avoidable via IBC), the overlapping control schemes are as efficient as an open-loop optimal control solution (with perfect model knowledge and demand prediction) developed for the same problem by Malekzadeh et al. (2021a) using a convex QP problem formulation; and as efficient as the centralized LQR. On the other hand, for the more challenging case of the congested scenario (where congestion may be mitigated, but cannot be fully avoided via IBC), the LMI-based approach (ii) performs better than the contractible controller (i), as it takes into account the whole system in the design phase.

Ongoing work considers application of the methods in microscopic simulation studies with vehicles moving in a lane-free environment, based on appropriate CAV movement strategies that have been developed in the frame of the Trafficfluid project (Yanumula et al., 2021; Malekzadeh et al. 2022).

Acknowledgements

The research leading to these results has received funding from the European Research Council under the European Union's Horizon 2020 Research and Innovation programme/ ERC Grant Agreement n. [833915], project TrafficFluid.

References

Ahmadi, A. and Aldeen, M., (2017). Robust overlapping load frequency output feedback control of multi-area interconnected power systems. *International Journal of Electrical Power & Energy Systems*, *89*, pp.156-172.

Bakule, L., (2014). Decentralized control: Status and outlook. *Annual Reviews in Control*, *38*(1), pp.71-80.

Bakule, L., Rodellar, J. and Rossell, J.M., (2006). Robust overlapping guaranteed cost control of uncertain state-delay discrete-time systems. *IEEE Transactions on Automatic Control*, *51*(12), pp.1943-1950.

Daganzo, C.F. (1994). The cell transmission model: A dynamic representation of highway traffic consistent with the hydrodynamic theory. *Transportation Research Part B: Methodological*, *28*(4), 269–287.

Datta, B. (2004). *Numerical methods for linear control systems* (Vol. 1). Academic Press.

Siljak, D.D., (2011). *Decentralized control of complex systems*. Courier Corporation.

Diakaki, C., Papageorgiou, M., Papamichail, I. & Nikolos, I. (2015). Overview and analysis of vehicle automation and communication systems from a motorway traffic management perspective. *Transportation Research Part A: Policy and Practice, 75*, 147–165.

Ferrara, A., Sacone, S. and Siri, S., (2018). *Freeway traffic modelling and control*. Berlin: Springer.

Hafeez, A., Shamair, Z., Shezad, N., Javed, F., Fazal, T., ur Rehman, S., Bazmi, A.A. and Rehman, F., 2021. Solar powered decentralized water systems: a cleaner solution of the industrial wastewater treatment and clean drinking water supply challenges. *Journal of Cleaner Production*, *289*, p.125717.

Hug-Glanzmann, G. and Andersson, G., (2009). Decentralized optimal power flow control for overlapping areas in power systems. *IEEE Transactions on Power Systems*, *24*(1), pp.327-336.

İftar, A. & Özgüner, Ü. (1990). Contractible controller design and optimal control with state and input inclusion. *Automatica, 26*(3), 593–597.

Ikeda, M., Šiljak, D.D. & White, D.E. (1981). Decentralized control with overlapping information sets. *Journal of Optimization Theory and Applications, 34*(2), 279–310.

Kontorinaki, M., Spiliopoulou, A., Roncoli, C., & Papageorgiou, M. (2017). First-order traffic flow models incorporating capacity drop: Overview and real-data validation. *Transportation Research Part B: Methodological, 106*, 52–75.

Kurzhanskiy, A.A. & Varaiya, P. (2010). Active traffic management on road networks: a macroscopic approach. *Philosophical Transactions of the Royal Society A: Mathematical, Physical and Engineering Sciences, 368*(1928), 4607–4626.

Malekzadeh, M., Manolis, D., Papamichail, I. and Papageorgiou, M., 2022, October. Empirical investigation of properties of lane-free automated vehicle traffic. In *2022 IEEE 25th International Conference on Intelligent Transportation Systems (ITSC)* (pp. 2393-2400). IEEE.

Malekzadeh, M., Papamichail, I. & Papageorgiou, M. (2021b). Linear–Quadratic regulators for internal boundary control of lane-free automated vehicle traffic. *Control Engineering Practice, 115*, Article 104912.

Malekzadeh, M., Papamichail, I., Papageorgiou, M. & Bogenberger, K. (2021a). Optimal internal boundary control of lane-free automated vehicle traffic. *Transportation Research Part C: Emerging Technologies, 126*, Article 103060.

Papageorgiou, M., Diakaki, C., Dinopoulou, V., Kotsialos, A. & Wang, Y. (2003). Review of road traffic control strategies. *Proceedings of the IEEE, 91*(12), 2043–2067.

Papageorgiou, M., Mountakis, K.S., Karafyllis, I., Papamichail, I. & Wang, Y. (2021). Lane-free artificial-fluid concept for vehicular traffic. *Proceedings of the IEEE, 109*(2), 114–121.

Papamichail, I., Bekiaris-Liberis, N., Delis, A.I., Manolis, D., Mountakis, K.S., Nikolos, I.K., Roncoli, C. and Papageorgiou, M., (2019). Motorway traffic flow modelling, estimation and control with vehicle automation and communication systems. *Annual Reviews in Control, 48*, pp.325-346.

Patil, B.V., Sampath, L.P.M.I., Krishnan, A. and Eddy, F.Y., (2019). Decentralized nonlinear model predictive control of a multimachine power system. *International Journal of Electrical Power & Energy Systems, 106*, pp.358-372.

Pasquale, C., Sacone, S., Siri, S. and Ferrara, A., 2020. Hierarchical centralized/decentralized event-triggered control of multiclass traffic networks. *IEEE Transactions on Control Systems Technology*, *29*(4), pp.1549-1564.

Toh, K.C., Todd, M.J. & Tütüncü, R.H. (1999). SDPT3 – A MATLAB software package for semidefinite programming, version 1.3. *Optimization Methods and Software*, *11*(1-4), 545–581.

Trudnowski, D.J. and Pierre, D.A., (1992). Decentralized indirect adaptive control scheme applicable to overlapping interconnected systems. *International Journal of Control*, *55*(2), pp.343-360.

VanAntwerp, J.G. & Braatz, R.D. (2000). A tutorial on linear and bilinear matrix inequalities. *Journal of Process Control*, *10*(4), 363–385.

Yanumula, V.K., Typaldos, P., Troullinos, D., Malekzadeh, M., Papamichail, I. & Papageorgiou, M. (2021). Optimal path planning for connected and automated vehicles in lane-free traffic. In *2021 IEEE International Intelligent Transportation Systems Conference* (pp. 3545–3552).

Yuan, K., Knoop, V. L., & Hoogendoorn, S. P. (2015). Capacity drop: Relationship between speed in congestion and the queue discharge rate. *Transportation Research Record*, 2491(1), 72–80.

Zečević, A.I. & Šiljak, D.D. (2005). A new approach to control design with overlapping information structure constraints. *Automatica*, *41*(2), 265–272.